RSC Advances

PAPER

View Article Online
View Journal | View Issue

Cite this: *RSC Adv.*, 2025, **15**, 30456

Pyomelanin-powered whole-cell biosensor for ultrasensitive and selective detection of bioavailable Hg(II)

Jiangpeng Tang,†[ab] Chang-ye Hui, †*[b] Shunyu Hu,[ab] Wanyan Wu,[ab] Peishuo Cao,[ab] Jingwen Ling,[bc] Xueqin Yang,[b] Zhenlie Huang *[a] and Yan Guo*[ad]

Rapid, low-cost trace inorganic Hg(II) detection in environmental waters remains a critical public-health challenge. Here, we engineered *Escherichia coli* into a naked-eye whole-cell biosensor by coupling a redesigned MerR-P*mer* element to the pyomelanin biosynthetic pathway. Three 4-hydroxyphenylpyruvate dioxygenase (HppD) homologs from *Aeromonas media* WS, *Aeromonas hydrophila* 4AK4, and *Pseudomonas aeruginosa* PAO1 were codon-optimized and functionally screened. The sensor strain of TOP10/pHg-PAO1 exhibited the broadest quantitative range (4.9–1250 nM) and the lowest detection limit (1.2 nM), outperforming most fluorescent counterparts. The water-soluble red-brown pyomelanin product was measured directly in the culture supernatants by absorbance at 400 nm, without requiring extraction. It remained chromogenically stable for at least 14 hours. The biosensor demonstrated absolute selectivity for Hg(II) in the presence of other ions, including Mg(II), Ca(II), Cd(II), Mn(II), Cu(II), Pb(II), and Zn(II), all at a concentration of 5 μM. It retained quantitative accuracy in tap, lake, and coastal seawater matrices. These features enable on-site, equipment-free screening of environmental waters and establish pyomelanin as a robust, user-friendly chromogenic reporter for next-generation whole-cell sensors.

Received 21st July 2025
Accepted 20th August 2025

DOI: 10.1039/d5ra05253j

rsc.li/rsc-advances

Introduction

Persistent mercury (Hg) is a globally distributed toxicant. Once released into the environment, Hg persists for decades and accumulates preferentially in aquatic systems—rivers, lakes, coastal waters, and tap-water distribution networks.[1] The World Health Organization (WHO) and the United States Environmental Protection Agency (USEPA), therefore, enforce stringent limits for inorganic Hg(II) in drinking water (6 ppb, ~30 nM) and surface waters (0.5–2 ppb, 2.5–10 nM).[2] Continuous surveillance at or below these low-nanomolar thresholds is crucial, yet challenging because conventional laboratory instrumentation (cold-vapour atomic fluorescence spectrometry, *etc.*) is costly, labour-intensive, and poorly suited to on-site screening.[3]

To overcome these limitations, biosensors offer a promising low-cost detection method as an alternative to traditional instrumental techniques.[4,5] Whole-cell biosensors that leverage natural mercuric resistance systems, particularly the mer operon, have emerged as miniaturized, reagent-free options.[6] In canonical designs, an Hg(II)-responsive MerR transcription factor drives expression of fluorescent or bioluminescent reporters upon Hg(II) binding, converting biological information into optical signals.[7–9] Although these devices achieve high sensitivity in buffered media, their deployment in environmental waters is hindered by two bottlenecks: (i) fluorescence or luminescence readouts require benchtop detectors equipped with specific excitation wavelengths and dedicated fluorescence-capture optics; (ii) the attainable limits of detection (LOD) often equal or exceed the regulatory thresholds for environmental waters, resulting in false negatives. There is an urgent need for reporter systems that combine high sensitivity at nanomolar concentration levels with visible color changes and long-term stability.

Pigment-based whole-cell sensors offer a promising solution. Violacein, carotenoid, and anthocyanin pathways have been engineered to produce intensely colored products that are quantifiable by simple absorbance or smartphone colorimetry.[10–12] Compared with fluorescent proteins, these chromogenic systems benefit from enzymatic signal amplification. However, lipophilic pigments such as violacein require organic extraction,[13] whereas water-soluble anthocyanins and indigoidine are prone to rapid oxidation and colour fading under environmental conditions.[11,14] Hence, an ideal chromogenic reporter should be water-soluble, chemically inert, and continuously synthesised to maintain colour stability.

[a]*Department of Toxicology, School of Public Health, Southern Medical University, Guangzhou 510515, China. E-mail: huangzhenlie858252@smu.edu.cn; yanguo615@163.com*

[b]*Department of Pathology & Toxicology, Shenzhen Prevention and Treatment Center for Occupational Diseases, Shenzhen 518020, China. E-mail: hcy_sypu@hotmail.com*

[c]*School of Public Health, Shenzhen University, Shenzhen 518055, China*

[d]*National Key Clinical Specialty of Occupational Diseases, Shenzhen Prevention and Treatment Center for Occupational Diseases, Shenzhen 518020, China*

† Jiangpeng Tang and Chang-ye Hui contributed equally to this work.

Pyomelanin—a water-soluble, red-brown pigment—fits these criteria. Its biosynthesis begins with tyrosine, which is transaminated to 4-hydroxyphenylpyruvate (4-HPP) by endogenous TyrB/AspC aminotransferases. 4-HPP is then converted to homogentisate (HGA) by 4-hydroxyphenylpyruvate dioxygenase (HppD), followed by spontaneous oxidation and polymerisation to pyomelanin.[15] Each HppD molecule can turn over multiple substrates to generate a polymeric pigment, lowering the LOD. Significantly, the entire pathway can be reconstituted in *Escherichia coli* (*E. coli*) with a single heterologous *hppD* gene, as substrates and cofactors are naturally present.[15,16] Comparative genomics reveals that although many environmental bacteria harbor HppD homologues, their catalytic efficiencies differ markedly.[17,18] Therefore, empirical screening of diverse HppD variants is necessary to maximize pigment output under sensor-relevant conditions.

Here, we harness the pyomelanin pathway to create a sensitive, selective, user-friendly whole-cell biosensor for inorganic Hg(II). By fusing a redesigned MerR-P*mer* regulatory module with codon-optimized *hppD* genes from *Aeromonas media* WS, *Aeromonas hydrophila* 4AK4, and *Pseudomonas aeruginosa* PAO1, we obtained sensor strains that produce water-soluble pyomelanin in direct proportion to extracellular Hg(II). The lead construct, TOP10/pHg-PAO1, achieved an LOD of 1.2 nM—well below the WHO drinking-water guideline—and retained quantitative accuracy in tap, lake, and seawater matrices. The oxidatively polymerized pigment remained chromogenically stable for >14 h, eliminating the extraction and fading issues that plague existing chromogenic reporters. These results demonstrate that pyomelanin-based whole-cell sensors can bridge the gap between ultra-sensitive laboratory methods and field-deployable environmental monitoring.

Materials and methods

Bacteria, vectors, and reagents

The bacterial strains and plasmids used in this study are listed in Table 1, and the corresponding gene and protein sequences are provided in Table S1. HppD homologs derived from *Aeromonas media* WS (GenBank: AHX61354.1), *Aeromonas hydrophila* 4AK4 (GenBank: AHE49923.1), and *Pseudomonas aeruginosa* PAO1 (GenBank: WKE27039.1) were selected for catalytic activity evaluation. The coding sequences of these three HppD homologs were codon-optimized for *E. coli*, synthesized by Sangon Biotech (Shanghai, China), and cloned into the *Nde*I and *Sac*I sites of pET-21a, yielding plasmids pET-WS, pET-4AK4, and pET-PAO1, respectively. These plasmids were chemically transformed into *E. coli* BL21(DE3) for protein expression validation.

To construct Hg(II)-responsive biosensors, a redesigned, decoupled mercuric-responsive element (MerR-P*mer*) was inserted as a *Bgl*II-*Xba*I fragment into pET-WS, pET-4AK4, and pET-PAO1, generating pHg-WS, pHg-4AK4, and pHg-PAO1, respectively. The resulting plasmids were transformed into *E. coli* TOP10 by chemical methods, and the recombinant strains served as sensor cells.

Recombinant *E. coli* were cultivated in LB medium (5 g L^{-1} yeast extract, 10 g L^{-1} tryptone, 10 g L^{-1} NaCl) supplemented with 50 μg mL^{-1} ampicillin at 30 °C and 250 rpm. Stock solutions of Hg(II), Pb(II), Cd(II), Zn(II), Mg(II), Cu(II), Mn(II), and Ca(II) were freshly prepared with analytical-grade salts (Aladdin, Shanghai) in ultrapure water.

Heterologous expression of HppD homologs in *E. coli*

Plasmids pET-WS, pET-4AK4, and pET-PAO1 were individually transformed into chemically competent *E. coli* BL21(DE3) cells. Single colonies from fresh LB-agar plates (50 μg mL^{-1} ampicillin) were inoculated into 3 mL LB medium and incubated overnight at 37 °C with shaking (250 rpm). Overnight cultures were diluted 1 : 100 into 15 mL fresh LB medium and grown under identical conditions until the early exponential phase. Recombinant protein expression was induced by adding IPTG to a final concentration of 1 mM, followed by 4 h incubation at 37 °C and 250 rpm. Cells were harvested by centrifugation (8000×*g*, 10 min, 4 °C), washed twice with ice-cold phosphate-buffered saline, and resuspended in lysis buffer (50 mM Tris-HCl pH 8.0, 150 mM NaCl). After sonication on ice (3 × 30 s,

Table 1 Bacterial strains and plasmids used in this study

Strains and plasmids	Genotypes or description	Reference
***E. coli* strains**		
TOP10	F^- *Φ*80 *lac*ZΔM15 Δ*lac*X74 *rec*A1	Invitrogen
BL21(DE3)	F^- *ompT hsdS*$_B$ (r_B^- m_B^-) *gal dcm* (DE3)	Merck
Plasmids		
pET-WS	pET-21a derivative containing the *hppD* gene from *Aeromonas media* WS cloned into *Nde*I and *Sac*I sites	This study
pET-4AK4	pET-21a derivative containing the *hppD* gene from *Aeromonas hydrophila* 4AK4 cloned into *Nde*I and *Sac*I sites	This study
pET-PAO1	pET-21a derivative containing the *hppD* gene from *Pseudomonas aeruginosa* PAO1 cloned into *Nde*I and *Sac*I sites	This study
pHg-WS	pET-WS derivative containing a redesigned Hg(II)-sensory element cloned into *Bgl*II and *Xba*I sites	This study
pHg-4AK4	pET-4AK4 derivative containing a redesigned Hg(II)-sensory element cloned into *Bgl*II and *Xba*I sites	This study
pHg-PAO1	pET-PAO1 derivative containing a redesigned Hg(II)-sensory element cloned into *Bgl*II and *Xba*I sites	This study

40% amplitude, 50% duty cycle), lysates were clarified by centrifugation (12 000×*g*, 20 min, 4 °C). Total protein, soluble, and inclusion fractions were analyzed by 10% SDS-PAGE followed by Coomassie Brilliant Blue R-250 staining.

Optimization of pyomelanin biosynthesis induction

For kinetic and dose–response studies, single colonies of TOP10/pHg-4AK4, TOP10/pHg-PAO1, and TOP10/pHg-WS were inoculated into 3 mL LB medium containing 50 μg mL^{-1} ampicillin and incubated overnight (37 °C, 250 rpm, 12 h). Overnight cultures were diluted 1 : 100 into fresh LB medium and grown for 3 h to the early exponential phase. Hg(II) stocks were then added to final concentrations of 0, 9.8, or 156.3 nM, and incubation continued at 30 °C, 250 rpm. At 2 h intervals (0–14 h), 1 mL samples were collected and stored at 4 °C. After completion of the time-course, 100 μL of each sample was transferred to a 96-well plate for optical density measurement at 600 nm (OD_{600}, bacterial density). The remaining 900 μL was centrifuged (12 000×*g*, 5 min), and 100 μL of the supernatant was transferred to a fresh 96-well plate to quantify pyomelanin accumulation by measuring absorbance at 400 nm.

Dose–response profiling of pyomelanin-based Hg(II) biosensors

Single colonies of TOP10/pHg-WS, TOP10/pHg-4AK4, and TOP10/pHg-PAO1 were inoculated into 3 mL LB medium containing 50 μg mL^{-1} ampicillin and cultured overnight (37 °C, 250 rpm, 12 h). Overnight cultures were diluted 1 : 100 into fresh LB medium (same antibiotic) and incubated for 3 h to the early exponential phase. Hg(II) stock solutions were then added by two-fold serial dilution[19] to 1 mL aliquots in 15 mL tubes to final concentrations of 0, 0.3, 0.6, 1.2, 2.4, 4.9, 9.8, 19.5, 39.1, 78.1, 156.3, 312.5, 625, 1250, 2500, and 5000 nM. Cultures were incubated at 30 °C, 250 rpm for 6 h.

For each tube, 100 μL was used to determine bacterial density at OD_{600}. The remaining 900 μL was centrifuged (12 000×*g*, 5 min), and 100 μL of the supernatant was transferred to a 96-well plate. Absorption spectra (350–750 nm) were recorded with a microplate reader (BioTek Epoch, USA) at 2 nm intervals, and the absorbance at 400 nm was used as the quantitative measure of pyomelanin accumulation.

Metal selectivity assay of TOP10/pHg-PAO1

A single colony of TOP10/pHg-PAO1 was inoculated into 3 mL fresh LB medium containing 50 μg mL^{-1} ampicillin and cultivated overnight (37 °C, 250 rpm, 12 h). Overnight cultures were diluted 1 : 100 into fresh LB medium (same antibiotic) and grown for 3 h to an early exponential phase. Individual metal ions—Mg(II), Ca(II), Cd(II), Mn(II), Cu(II), Pb(II), Zn(II), and Hg(II)—were then added to final concentrations of 5, 2.5, and 1.25 μM, respectively. Cultures were incubated at 30 °C, 250 rpm for 6 h. A no-metal control was included under identical conditions.

Following incubation, 100 μL of each culture was used to determine bacterial density at OD_{600}. The remaining 900 μL was centrifuged (12 000×*g*, 5 min), and 100 μL of the supernatant was transferred to a 96-well plate to measure pyomelanin absorbance at 400 nm.

Interference evaluation of TOP10/pHg-PAO1

A single colony of TOP10/pHg-PAO1 was inoculated into 3 mL LB medium supplemented with 50 μg mL^{-1} ampicillin and grown overnight (37 °C, 250 rpm, 12 h). Overnight cultures were diluted 1 : 100 into fresh LB medium (identical antibiotics) and incubated to the early exponential phase. Thereafter, stock solutions of Mg(II), Ca(II), Cd(II), Mn(II), Cu(II), Pb(II), and Zn(II) were added to final concentrations of 5 μM or 2.5 μM, respectively. At the same time, Hg(II) was maintained at a constant, sub-toxic concentration of 50 nM. Cultures were then incubated at 30 °C, 250 rpm for 6 h.

After incubation, 100 μL of each sample was used to determine bacterial density at OD_{600}. The remaining 900 μL was centrifuged (12 000×*g*, 5 min, 4 °C), and 100 μL of the supernatant was transferred to a 96-well plate for measurement of pyomelanin absorbance at 400 nm.

Hg(II) response of TOP10/pHg-PAO1 in environmental water matrices

Environmental water samples were collected from four sources: laboratory-grade deionized water, municipal tap water, surface water from Xianhu Lake (Luohu District, Shenzhen, Guangdong, China), and seawater from Daya Bay (Yantian District, Shenzhen, Guangdong, China). Samples were clarified by centrifugation (10 000×*g*, 10 min) and sterilized through a 0.22 μm membrane filter (Millipore, Billerica, MA, USA).[20] Detection media were prepared according to the ratios specified in Table 2.

Overnight cultures of TOP10/pHg-PAO1 were inoculated at 1% (v/v) into each medium containing 50 μg mL^{-1} ampicillin and incubated at 30 °C, 250 rpm for 3 h to reach the early exponential phase. Hg(II) was then added by two-fold serial dilution to final concentrations of 0, 19.5, 39.1, 78.1, 156.3, 312.5, 625, and 1250 nM, followed by a 6 h incubation at 30 °C, 250 rpm. As described above, bacterial density (OD_{600}) and pyomelanin accumulation (A_{400}) were measured.

Results and discussion

Differential soluble expression of three HppD homologs in *E. coli*

The pET-21a vector was used to construct IPTG-inducible expression cassettes for the three HppD homologs (Fig. 1A).

Table 2 Detection culture system for different environmental water samples

Component	Deionized water	Tap water	Surface water	Seawater
Water samples	90%	90%	90%	50%
10 × LB	10%	10%	10%	—
10 × NaCl-free LB	—	—	—	10%
Sterile water	—	—	—	40%

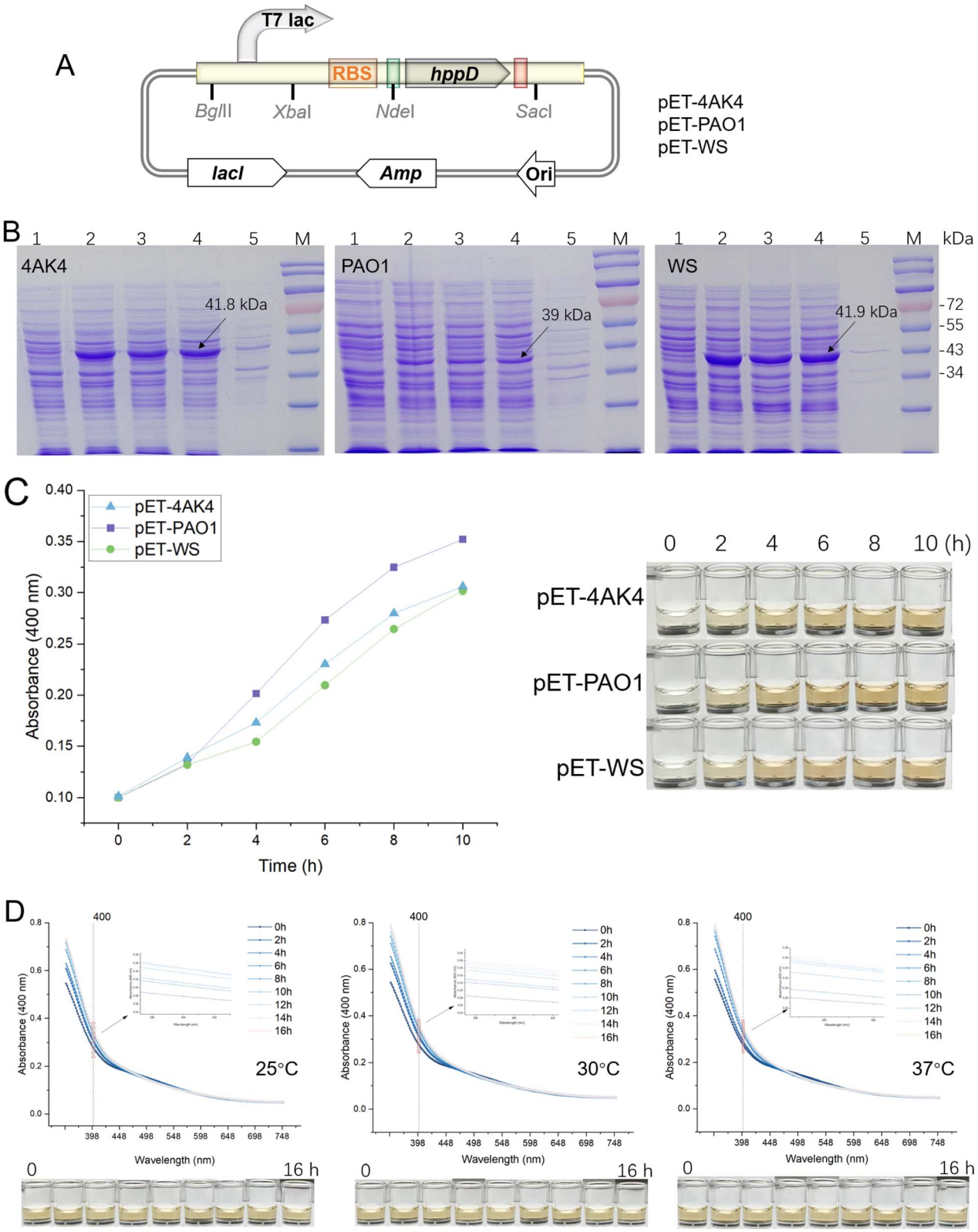

Fig. 1 Heterologous expression of HppD homologs in *E. coli* BL21(DE3). (A) Schematic representation of pET-21a-derived expression cassettes for 4AK4, PAO1, and WS HppD homologs. (B) Representative 10% SDS-PAGE analysis (lanes left to right): 1, uninduced total protein; 2, IPTG-induced total protein; 3, post-sonication lysate; 4, soluble fraction; 5, insoluble pellet; M, protein marker. (C) Absorption spectra (left) and photographs of the supernatant (right) of BL21(DE3)/pET-4AK4, BL21(DE3)/pET-PAO1, and BL21(DE3)/pET-WS after IPTG induction. The experiment was repeated three times, and this is a representative result. (D) Absorption spectra of the BL21(DE3)/pET-PAO1 supernatant at three different temperatures over 0–16 h after IPTG induction.

After IPTG induction, SDS-PAGE revealed that all three recombinant proteins migrated at the predicted molecular masses (Table S1). The band intensity analysis of 10% SDS-PAGE showed that HppD-4AK4 and HppD-WS were highly expressed, whereas HppD-PAO1 was expressed at lower levels (Fig. 1B). Importantly, the majority of each recombinant protein was recovered in the soluble fraction after sonication, indicating practical soluble expression.

The three selected HppD proteins originate from pyomelanin-producing strains[18,21] and share 88–99% pairwise identity (Fig. S1). Notably, the 4AK4 and WS homologs differ by only eight residues. However, both accumulate to high levels in *E. coli* (Fig. 1B). In contrast, PAO1 deviates by >30 residues from 4AK4/WS and exhibits markedly lower expression despite employing the same expression conditions. These data highlight that even closely related homologs can display pronounced expression heterogeneity in a heterologous host. Therefore, empirical screening of HppD variants is essential for maximizing pyomelanin output in engineered strains.

We further sampled the supernatants of BL21(DE3)/pET-4AK4, BL21(DE3)/pET-PAO1, and BL21(DE3)/pET-WS at 2 hour intervals over 10 hours after induction with 1 mM IPTG during the early exponential growth phase and measured the absorbance at 400 nm. As shown in Fig. 1C, BL21(DE3)/pET-PAO1 exhibited more substantial pigment accumulation compared to BL21(DE3)/pET-WS and BL21(DE3)/pET-4AK4, while the latter two showed similar levels of pigment accumulation. Considering that HppD-PAO1 had lower protein expression but potentially higher catalytic activity, we further investigated the stability of pyomelanin produced by BL21(DE3)/pET-PAO1.

The supernatant containing pyomelanin from induced BL21(DE3)/pET-PAO1 was incubated at 25 °C, 30 °C, and 37 °C under natural light at 150 rpm for 16 hours, with samples taken every 2 hours to measure the absorption spectra (350–750 nm). As shown in Fig. 1D, the red-brown pyomelanin, resulting from the spontaneous oxidation and polymerization of homogentisate (HGA),[15] exhibited minimal changes in both absorption spectra and visual appearance over 16 hours at all three

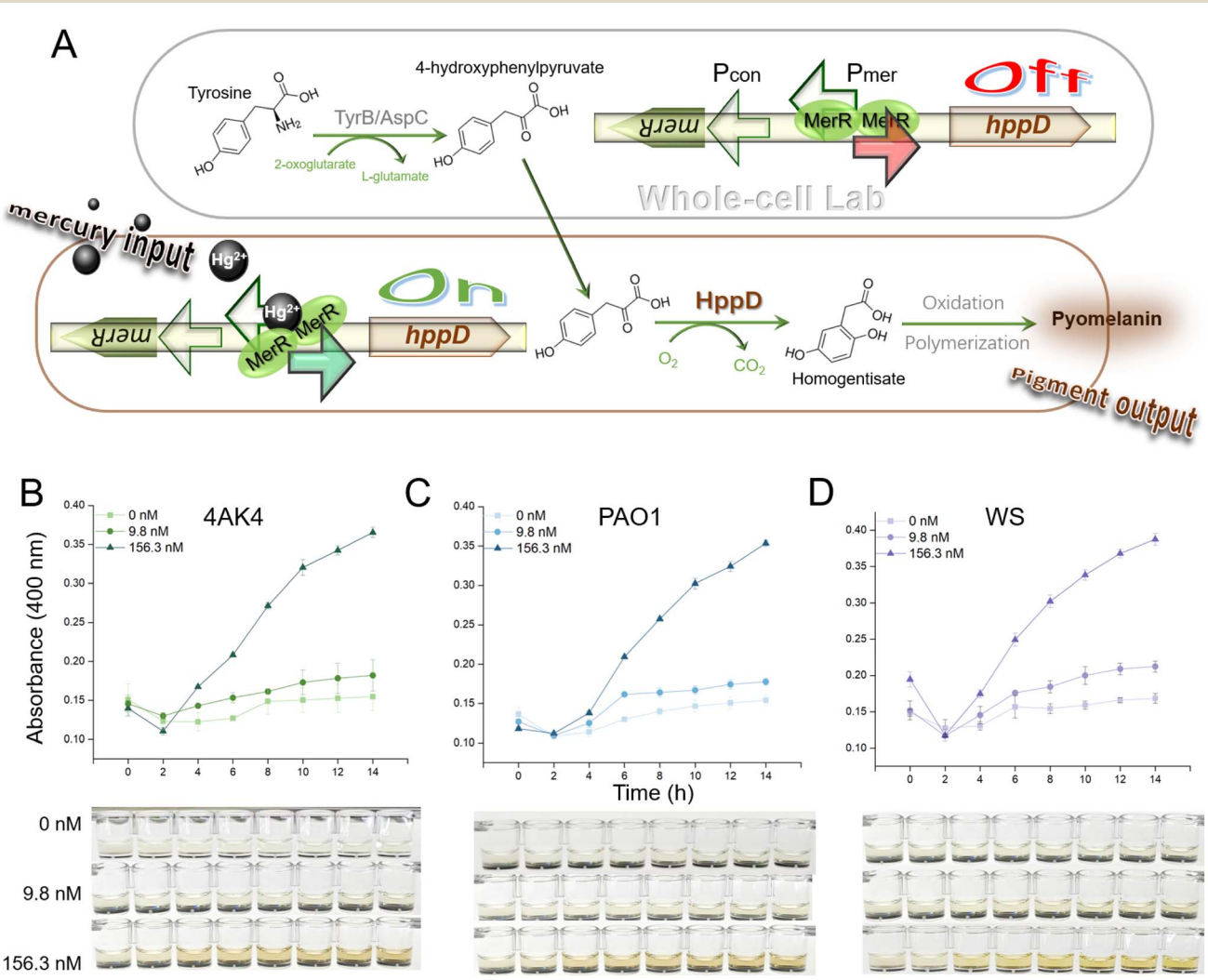

Fig. 2 Visual whole-cell Hg(II) biosensor design and kinetic response. (A) Schematic of the MerR-P*mer*-controlled pyomelanin pathway in *E. coli*. (B–D) Time-course A_{400} (top) and corresponding culture supernatant photographs (bottom) for TOP10/pHg-4AK4 (B), TOP10/pHg-PAO1 (C), and TOP10/pHg-WS (D) exposed to 0–156.3 nM Hg(II). Data are means ± SD ($n = 3$).

temperatures, indicating high stability. Unlike other water-soluble pigments, such as indigoidine,[14] pyomelanin is a product of a rapid oxidation process. Its color stability makes it an ideal chromogenic signal for sensing applications.

Hg(II)-dependent pyomelanin biosynthesis exhibits time- and dose-responsive behavior

A redesigned Hg(II)-sensory element was inserted upstream of the *hppD* gene (Fig. 2A). In the absence of Hg(II), dimeric MerR represses the *mer* promoter (P*mer*) by binding to the operator region, sequestering RNA polymerase, and preventing transcription initiation.[6] The MerR dimer acts as a specific repressor, recognizing and binding to a conserved DNA sequence within the operator region. This binding stabilizes a closed promoter complex, inhibiting the transcription of downstream genes.

Upon Hg(II) entry, the MerR dimer undergoes a conformational change upon binding to Hg(II) ions. This Hg(II)-induced conformational shift alters the DNA-binding affinity of MerR, causing it to open the operator region. The action of MerR allows RNA polymerase to bind to the promoter and initiate transcription of the *hppD* gene. This activation mechanism is specific to Hg(II) due to the unique metal-binding sites within the MerR protein, which enable selective recognition and binding of Hg(II) ions over other metal ions.[22]

The MerR-mediated activation of *hppD* transcription is a key step in the biosensor design, as it couples the presence of Hg(II) to the production of pyomelanin, a chromogenic reporter. This

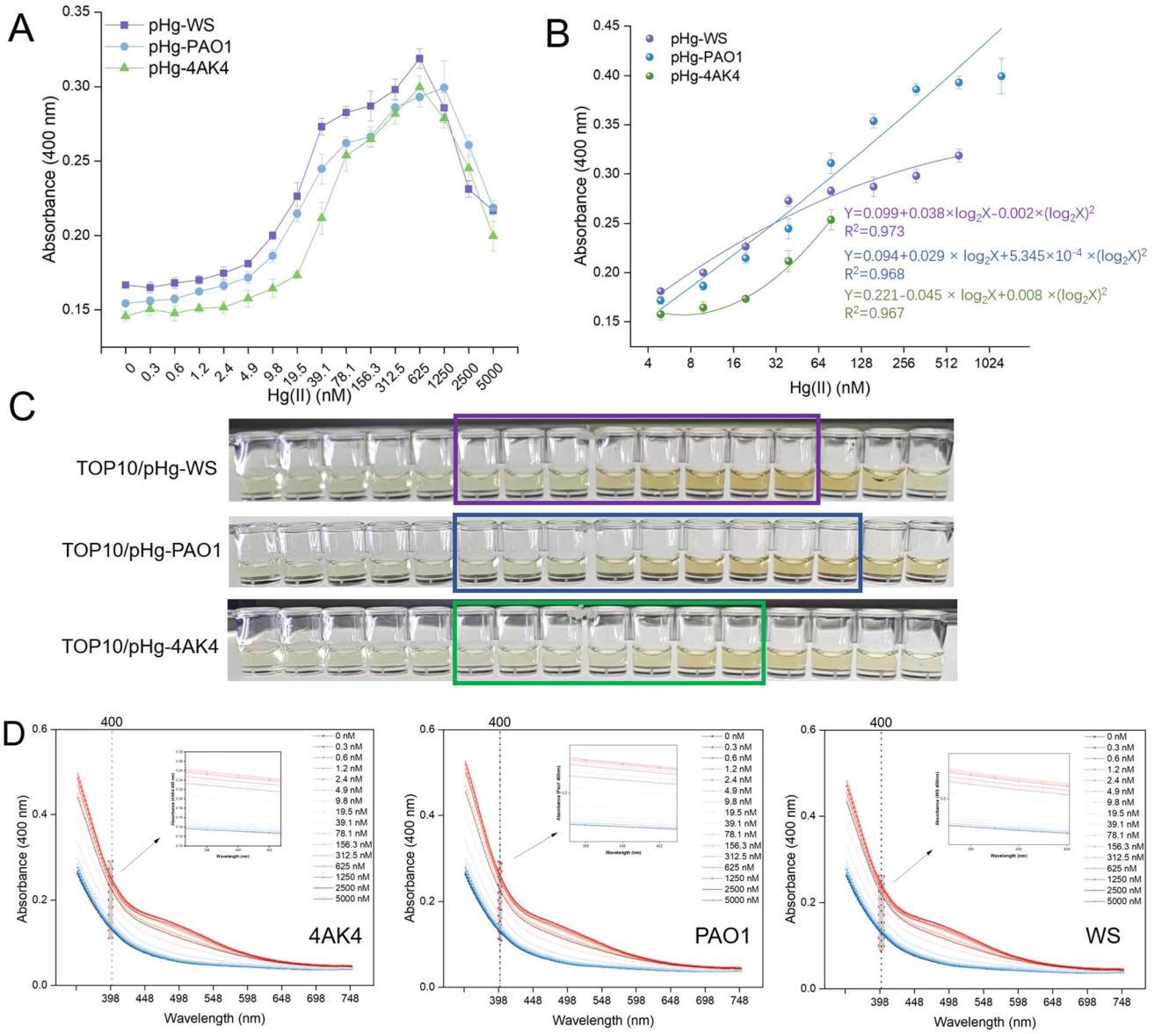

Fig. 3 Dose-dependent pyomelanin production in response to Hg(II). (A) A_{400} of culture supernatants *versus* Hg(II) concentration (mean ± SD, $n = 3$). (B) Non-linear regression curves for each biosensor. (C) In the representative photographs of supernatants after 6 h induction, shaded boxes indicate the quantifiable windows. (D) Representative visible-light absorption spectra of culture supernatant. A red dashed line highlights the 400 nm region.

biochemical mechanism ensures that pyomelanin synthesis is directly proportional to the concentration of Hg(II) in the environment, providing a quantitative and visible signal for Hg(II) detection.

Endogenous TyrB or AspC converts tyrosine to 4-hydroxyphenylpyruvate, which is subsequently oxidized by HppD to HGA. Spontaneous oxidation and polymerisation of HGA yield the characteristic red-brown pyomelanin,[15] whose accumulation is proportional to extracellular Hg(II) and enables naked-eye quantification.

All three biosensor strains exhibited comparable time–dose–response profiles (Fig. 2B–D). After 2 h of induction, A_{400} declined slightly, reflecting metabolic lag. From 4 h onwards, absorbance increased in a concentration-dependent manner. At 156.3 nM Hg(II), A_{400} increased sharply, and a visible red-brown color emerged within 4 h.

The catalytic divergence among the three HppD homologs can be attributed to differences in their amino acid sequences, which influence substrate binding and catalytic efficiency. Specifically, the sequence variations affect the active site configuration and substrate-enzyme fit, leading to differences in sensitivity and activity. Despite lower expression levels (Fig. 1B), HppD-PAO1 exhibited catalytic efficiency comparable to the higher-expressing 4AK4 and WS homologs (Fig. 2B). This is likely due to its unique active site residues, which enhance substrate binding and turnover. These relationships between sequence and function underscore the importance of empirical screening and optimization of HppD variants to achieve optimal pyomelanin production and sensor performance.

Quantitative Hg(II) detection using red-brown pyomelanin as a chromogenic reporter

Fig. S2 confirms that ≤5 μM Hg(II) exerted no detectable cytotoxicity on any sensor strain. All three biosensors exhibited a bell-shaped dose–response curve over 0–5000 nM (Fig. 3A), with maximal pigment accumulation followed by attenuation at supra-optimal concentrations. TOP10/pHg-4AK4 and TOP10/pHg-WS peaked around 625 nM and yielded robust non-linear regressions within 4.9–64 nM ($R^2 = 0.967$) and 4.9–625 nM ($R^2 = 0.973$), respectively (Fig. 3B). Statistically significant increases over background (Student's t-test, $P < 0.05$) were first observed at 4.9 nM for 4AK4 and 2.4 nM for WS.

In contrast, TOP10/pHg-PAO1, despite the lowest expression level (Fig. 1B), displayed the broadest dynamic range (4.9–1250 nM, $R^2 = 0.968$) and the lowest limit of detection (LOD = 1.2 nM). LOD and quantitative range outperform previously reported carotenoid- or violacein-based sensors,[13,23] and cover internationally accepted environmental mercury limits. The observed bell-shaped curve, which shows saturation above 1.25 μM Hg(II), may result from unoptimized MerR levels[24] or oxidative stress caused by pyomelanin accumulation.[17] Future work will explore strategies to mitigate these effects, such as optimizing MerR expression levels or incorporating antioxidant pathways, to further extend the dynamic range and enhance sensor performance for higher Hg(II) concentrations.

Visual inspection of the culture supernatants revealed a color change from pale yellow to intense red-brown with increasing Hg(II) concentration, following a "parabolic" trajectory (Fig. 3C). The absorbance spectra showed a monotonic

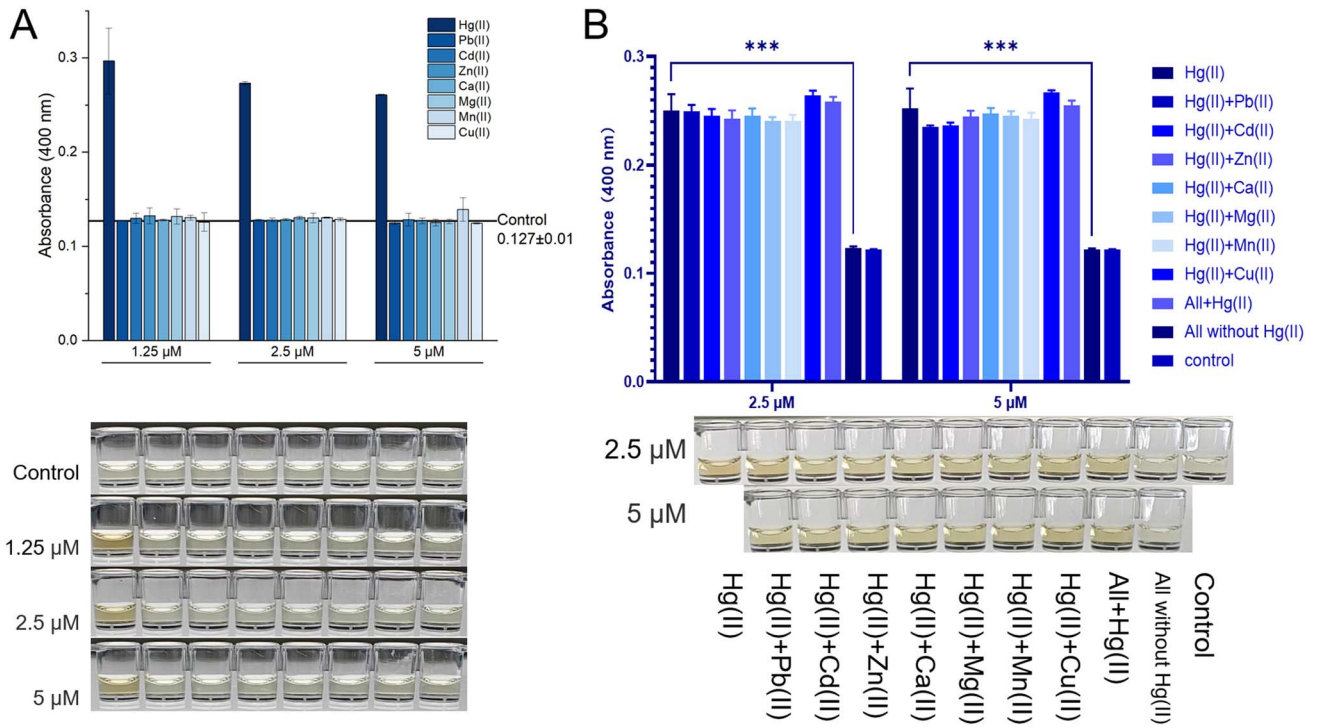

Fig. 4 Metal selectivity and anti-interference performance of TOP10/pHg-PAO1. (A) Pyomelanin production after exposure to 1.25, 2.5, and 5 μM of individual metal ions. The horizontal line represents the metal-free control (A_{400}). (B) Co-exposure to 50 nM Hg(II) plus 2.5 or 5 μM of the indicated metals; bars show mean ± SD ($n = 3$), ***$P < 0.001$. Representative photographs of supernatants are shown below each panel.

increase across the 350–700 nm range without distinct peaks,[21] confirming pyomelanin accumulation (Fig. 3D). This broad, featureless absorbance envelope aligns with prior studies[21] measuring the visible and infrared spectra of pyomelanin, further corroborating our spectral data and providing additional evidence for pyomelanin production in our system. The absorbance at 400 nm was chosen for quantification to minimize background interference from the LB medium at 600 nm. The trend of the absorbance spectra obtained from direct scans of the induced bacterial cultures (Fig. S3) was consistent with that of the supernatants after centrifugation (Fig. 3D), both showing an overall upward trend with increasing Hg(II) exposure concentration.

Thus, HppD-PAO1 couples high catalytic efficiency with superior sensitivity and a wide range, underscoring the importance of broad enzymatic screening when deploying pigment biosynthetic genes as reporters.

Metal selectivity and anti-interference performance of the selected biosensor TOP10/pHg-PAO1

When TOP10/pHg-PAO1 was challenged with sub-cytotoxic concentrations (1.25, 2.5 and 5 μM) of Mg(II), Ca(II), Cd(II), Mn(II), Cu(II), Pb(II), Zn(II) or Hg(II), only Hg(II) triggered a visible red-brown coloration and a significant increase in A_{400} (Fig. 4A). The remaining divalent cations produced responses indistinguishable from the metal-free control (horizontal line). Although pigment-based reporters can amplify non-specific signals, prior work indicates that the selectivity of MerR-based sensors is governed by the metal-binding specificity of dimeric MerR rather than the reporter itself.[25,26]

We examined whether co-occurring metals would interfere with Hg(II) detection to assess real-world applicability. TOP10/pHg-PAO1 was co-exposed to 50 nM Hg(II) plus 2.5 or 5 μM of each of the seven non-target metals. No significant growth inhibition was observed (Fig. S4). The presence of non-target metals did not alter the Hg(II)-induced response ($P > 0.05$) (Fig. 4B). Cultures lacking Hg(II) remained colorless and differed statistically from Hg(II)-only treatments ($P < 0.001$). At the same time, naked-eye discrimination was readily achieved (Fig. 4B). These findings confirm that dimeric MerR retains high Hg(II) specificity even in complex metal mixtures and that the tested ions do not inhibit HppD activity.

Robust quantitative detection of Hg(II) in diverse environmental water matrices

To examine real-world applicability, we challenged TOP10/pHg-PAO1 with Hg(II) in four different water matrices: deionized water, tap water, lake surface water, and coastal seawater. Samples were clarified (10 000×*g*, 10 min), sterilized (0.22 μm filtration), and incorporated at high ratios (90% for freshwater, 50% for seawater) to minimize dilution-related LOD elevation.[27,28] Under these conditions, bacterial growth remained

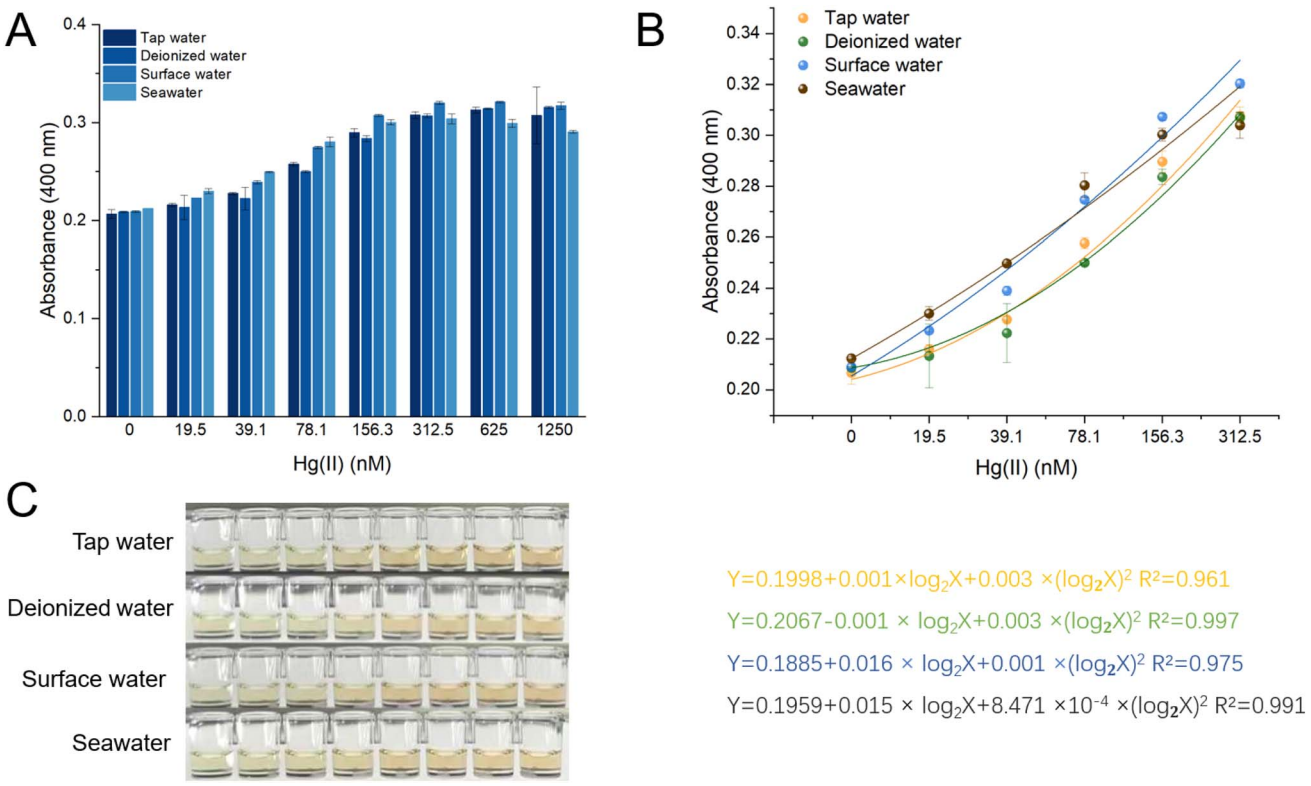

Fig. 5 Quantitative Hg(II) detection in environmental waters by TOP10/pHg-PAO1. (A) A_{400} after 6 h exposure to increasing Hg(II) in deionized water, tap water, surface water, and seawater (mean ± SD, $n = 3$). (B) Corresponding non-linear regression curves. (C) Representative photographs illustrating color gradients across matrices.

unimpaired (Fig. S5), and seawater cultures even showed slightly elevated cell densities.

Across all matrices, TOP10/pHg-PAO1 exhibited consistent dose–response behavior for 0–312.5 nM Hg(II) (Fig. 5A), demonstrating that dissolved organic matter or high ionic strength did not interfere with MerR-mediated Hg(II) recognition or HppD catalysis. Non-linear regression analyses yielded high coefficients of determination ($R^2 > 0.96$) for every matrix (Fig. 5B), and progressive darkening of culture supernatants was readily visible to the naked eye (Fig. 5C).

In this study, we successfully repurposed HppD homologues as chromogenic reporters. Using Hg(II) biosensing as a model, we demonstrated that pyomelanin synthesis affords a built-in signal amplification that enables nanomolar-level detection of Hg(II) with a broad quantitative range, outperforming previously reported fluorescent whole-cell biosensors.[6,24,29] As a water-soluble pigment, pyomelanin can be quantified directly in the culture supernatant, eliminating the need for organic solvent extraction required for lipophilic reporters such as violacein,[13] deoxyviolacein,[30] proviolacein,[31] prodeoxyviolacein,[32,33] and indigo.[34] Earlier studies have revealed that water-soluble colorants (*e.g.*, indigoidine, anthocyanins) are prone to air oxidation and rapid fading.[11,35] In contrast, pyomelanin is an oxidatively polymerized end-product. Here we show that it is continuously produced during fermentation and remains chromogenically stable in the culture medium, rendering it an ideal chromogenic reporter, making it highly suitable for on-site, real-time monitoring of Hg(II) pollution.

By screening multiple HppD homologues, we uncovered marked differences in catalytic efficiency. HppD-PAO1 exhibited the highest turnover activity. Future efforts will focus on enhancing HppD-PAO1 expression and refining fermentation parameters to improve color intensity for visual detection. Beyond mercury monitoring, this robust pyomelanin system holds promising potential for low-level promoter screening and designing next-generation whole-cell biosensors against a broad spectrum of environmental contaminants.

Conclusion

We herein report metabolic engineering of the pyomelanin pathway into a high-performance, whole-cell colorimetric biosensor for Hg(II). By coupling a Hg(II)-sensing MerR module with three distinct HppD homologues, we identified TOP10/pHg-PAO1 as the optimal sensor, achieving an ultralow detection limit (1.2 nM) and a quantitative range (4.9–1250 nM) that surpasses most existing fluorescent systems. The water-soluble red-brown pyomelanin permits direct, solvent-free quantification and is stable under prolonged fermentation, circumventing hydrophilic pigments' instability and lipophilic pigments' extraction bottlenecks. The sensor exhibits absolute selectivity for Hg(II) in environmentally relevant co-metals and retains robust performance across deionized, tap, surface, and seawater matrices. These attributes, combined with the simplicity of naked-eye readout and compatibility with standard microplate assays, make this platform an attractive alternative to instrumental methods for on-site Hg(II) screening. Extending the same framework to other pollutants or promoter libraries is feasible and warrants further exploration.

Conflicts of interest

There are no conflicts to declare.

Data availability

The data supporting this article have been included as part of the SI. See DOI: **https://doi.org/10.1039/d5ra05253j**.

Table S1: DNA and amino acid sequences of *hppD* genes and Hg(II)-responsive promoter elements used in the study. Fig. S1: Sequence alignment of HppD homologs. Fig. S2: Bacterial turbidity after Hg(II) exposure. Fig. S3: Absorption spectra of pyomelanin production in response to Hg(II). Fig. S4: Biosensor growth in mixed metal conditions. Fig. S5: Biosensor growth in different water matrices. See DOI: **https://doi.org/10.1039/d5ra05253j**.

Acknowledgements

This work was supported by the Natural Science Foundation of Shenzhen Municipality (JCYJ20220531091209022, JCYJ20230807151400002, JCYJ20240813162259005), the Natural Science Foundation of Guangdong Province (2023A1515011184, 2025A1515011667) and Shenzhen Key Medical Discipline Construction Fund (SZXK068).

References

1 D. Peng, Z. Tan, T. Yuan, P. Wu, Z. Song, P. Zhang, S. Huang, Y. Zhang, T. Lei, B. A. Middleton, J. E. Sonke, G. Lei and J. Gao, *Sci. Adv.*, 2025, **11**, eadw0471.
2 N. Okati, Z. Ebrahimi-Khusfi, S. Zandifar and R. Taghizadeh-Mehrjardi, *Environ. Geochem. Health*, 2025, **47**, 239.
3 J. Falandysz, A. R. Fernandes and H. Eun, *Adv. Appl. Microbiol.*, 2025, **130**, 1–122.
4 H.-B. Wang, Y. Chen, Y. Li, H.-D. Zhang and J.-T. Cao, *RSC Adv.*, 2015, **5**, 94099–94104.
5 H. B. Wang, H. Y. Bai, Y. S. Wang, T. Gan and Y. M. Liu, *Mikrochim. Acta*, 2020, **187**, 185.
6 C. Y. Hui, B. C. Ma, S. Y. Hu and C. Wu, *Environ. Pollut.*, 2024, **341**, 123016.
7 J. Wang, Q. Hu, C. Liu, Y. Feng, J. Zhu and H. Chen, *Biosens. Bioelectron.*, 2025, **287**, 117687.
8 K. Zhu, D. Chen, Y. Cai, T. Zhang, J. Ma, L. Bao, F. Zhao, L. Wu and S. Chen, *Environ. Sci. Technol.*, 2023, **57**, 16964–16973.
9 S. Cai, Y. Shen, Y. Zou, P. Sun, W. Wei, J. Zhao and C. Zhang, *Analyst*, 2018, **143**, 630–634.
10 C. Y. Hui, S. Y. Hu, X. Q. Yang and Y. Guo, *Mutat. Res., Genet. Toxicol. Environ. Mutagen.*, 2023, **888**, 503639.
11 Y. Guo, Z. L. Huang, D. L. Zhu, S. Y. Hu, H. Li and C. Y. Hui, *Front. Microbiol.*, 2022, **13**, 975421.
12 C. Y. Hui, S. Y. Hu, L. M. Li, J. P. Yun, Y. F. Zhang, J. Yi, N. X. Zhang and Y. Guo, *RSC Adv.*, 2022, **12**, 36142–36148.

13 C. Y. Hui, Y. Guo, L. Liu, N. X. Zhang, C. X. Gao, X. Q. Yang and J. Yi, *RSC Adv.*, 2020, **10**, 28106–28113.
14 C. Y. Hui, Y. Guo, L. M. Li, L. Liu, Y. T. Chen, J. Yi and N. X. Zhang, *Appl. Microbiol. Biotechnol.*, 2021, **105**, 6087–6102.
15 S. Singh, S. B. Nimse, D. E. Mathew, A. Dhimmar, H. Sahastrabudhe, A. Gajjar, V. A. Ghadge, P. Kumar and P. B. Shinde, *Biotechnol. Adv.*, 2021, **53**, 107773.
16 L. M. Martinez, A. Martinez and G. Gosset, *Front. Bioeng. Biotechnol.*, 2019, **7**, 285.
17 U. Perez-Cuesta, L. Aparicio-Fernandez, X. Guruceaga, L. Martin-Souto, A. Abad-Diaz-de-Cerio, A. Antoran, I. Buldain, F. L. Hernando, A. Ramirez-Garcia and A. Rementeria, *Int. Microbiol.*, 2020, **23**, 55–63.
18 H. Wang, Y. Qiao, B. Chai, C. Qiu and X. Chen, *PLoS One*, 2015, **10**, e0120923.
19 C. Y. Hui, Y. Guo, H. Li, Y. T. Chen and J. Yi, *Front. Microbiol.*, 2022, **13**, 846524.
20 Y. Guo, M. q. Liu, X. q. Yang, Y. y. Guo and C. y. Hui, *Appl. Environ. Microbiol.*, 2025, e0060125.
21 F. Bolognese, C. Scanferla, E. Caruso and V. T. Orlandi, *Int. J. Biol. Macromol.*, 2019, **133**, 1072–1080.
22 G. Tulin, N. R. Figueroa, S. K. Checa and F. C. Soncini, *Mol. Microbiol.*, 2024, **121**, 230–242.
23 Y. Guo, C. Y. Hui, L. Liu, M. P. Chen and H. Y. Huang, *Sci. Rep.*, 2021, **11**, 13516.
24 M. Guo, R. Du, Z. Xie, X. He, K. Huang, Y. Luo and W. Xu, *J. Biol. Eng.*, 2019, **13**, 70.
25 Y. Guo, B. C. Ma, W. Q. Zhang, B. X. Li, J. M. Ou, F. Liu and C. Y. Hui, *Ecotoxicol. Environ. Saf.*, 2025, **295**, 118157.
26 B. C. Ma, Y. Guo, Y. R. Lin, J. Zhang, X. Q. Wang, W. Q. Zhang, J. G. Luo, Y. T. Chen, N. X. Zhang, Q. Lu and C. Y. Hui, *Biosens. Bioelectron.*, 2024, **248**, 115961.
27 M. Q. Liu, Y. Guo, C. Wu, C. X. Gao, F. Liu and C. Y. Hui, *J. Hazard Mater.*, 2024, **477**, 135398.
28 C. Wu, Y. Guo, Y. X. Xie, S. Y. Hu, J. M. Ou, B. X. Li, N. X. Zhang and C. Y. Hui, *J. Hazard Mater.*, 2024, **480**, 136213.
29 X. Y. Liu, Y. Guo, W. Q. Zhang, J. Bai, B. C. Ma, L. T. Zhou and C. Y. Hui, *Environ. Res.*, 2025, **275**, 121418.
30 C. Y. Hui, Y. Guo, D. L. Zhu, L. M. Li, J. Yi and N. X. Zhang, *Biosens. Bioelectron.*, 2022, **214**, 114531.
31 D. L. Zhu, Y. Guo, B. C. Ma, Y. Q. Lin, H. J. Wang, C. X. Gao, M. Q. Liu, N. X. Zhang, H. Luo and C. Y. Hui, *Front. Microbiol.*, 2023, **14**, 1218933.
32 S.-Y. Hu, C.-Y. Hui, C. Wu, C.-X. Gao, Z. Huang and Y. Guo, *Ecol. Indic.*, 2024, **166**, 112244.
33 Y. Guo, D.-L. Zhu, M.-Q. Liu, Y.-T. Chen, S.-Y. Hu and C.-Y. Hui, *J. Environ. Chem. Eng.*, 2024, **12**, 114178.
34 Y. Guo, S. Y. Hu, C. Wu, C. X. Gao and C. Y. Hui, *ACS Omega*, 2024, **9**, 33868–33881.
35 C.-Y. Hui, Y. Guo, C.-X. Gao, H. Li, Y.-R. Lin, J.-P. Yun, Y.-T. Chen and J. Yi, *Environ. Technol. Innovat.*, 2022, **27**, 102511.